Supporting Information

for

Electrochemical Synthesis of NiCo Layered Double Hydroxide Nanosheets Decorated on Moderately Oxidized Graphene Film for High Performance Energy Storage

By Dedong Jia,‡[a] Degang Jiang,‡[a] Yiwei Zheng,[a] Hua Tan,[b] Xueying Cao,[a] Fang Liu,[a] Lijun Yue,[a] Yuanyuan Sun,[a] and Jingquan Liu *[a]*

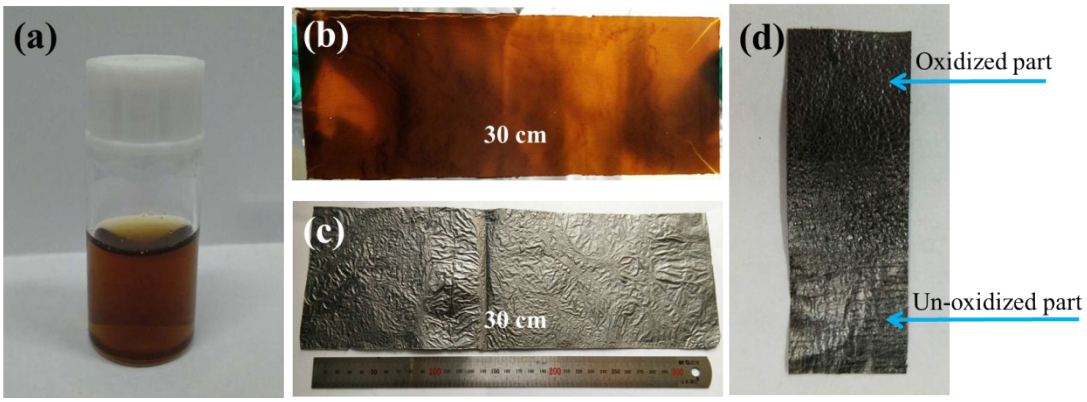

Figure S1 Photograph of the GO solution (a), GO film (b), RGO film (c) and partial oxidized RGO film.

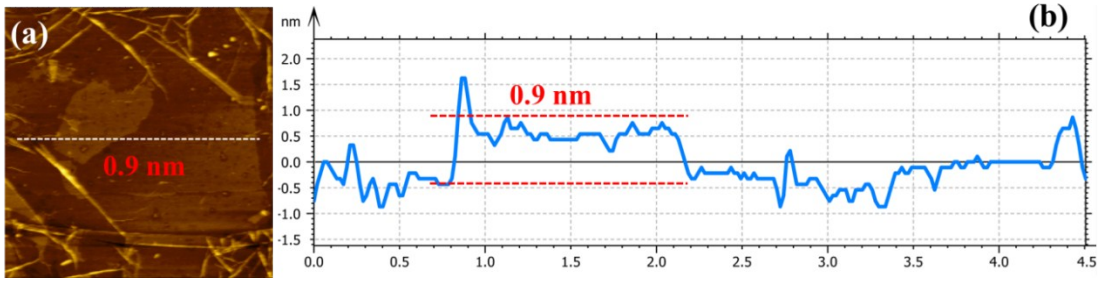

Figure S2 Tapping mode AFM images of the RGO films(a) with height profiles (b).

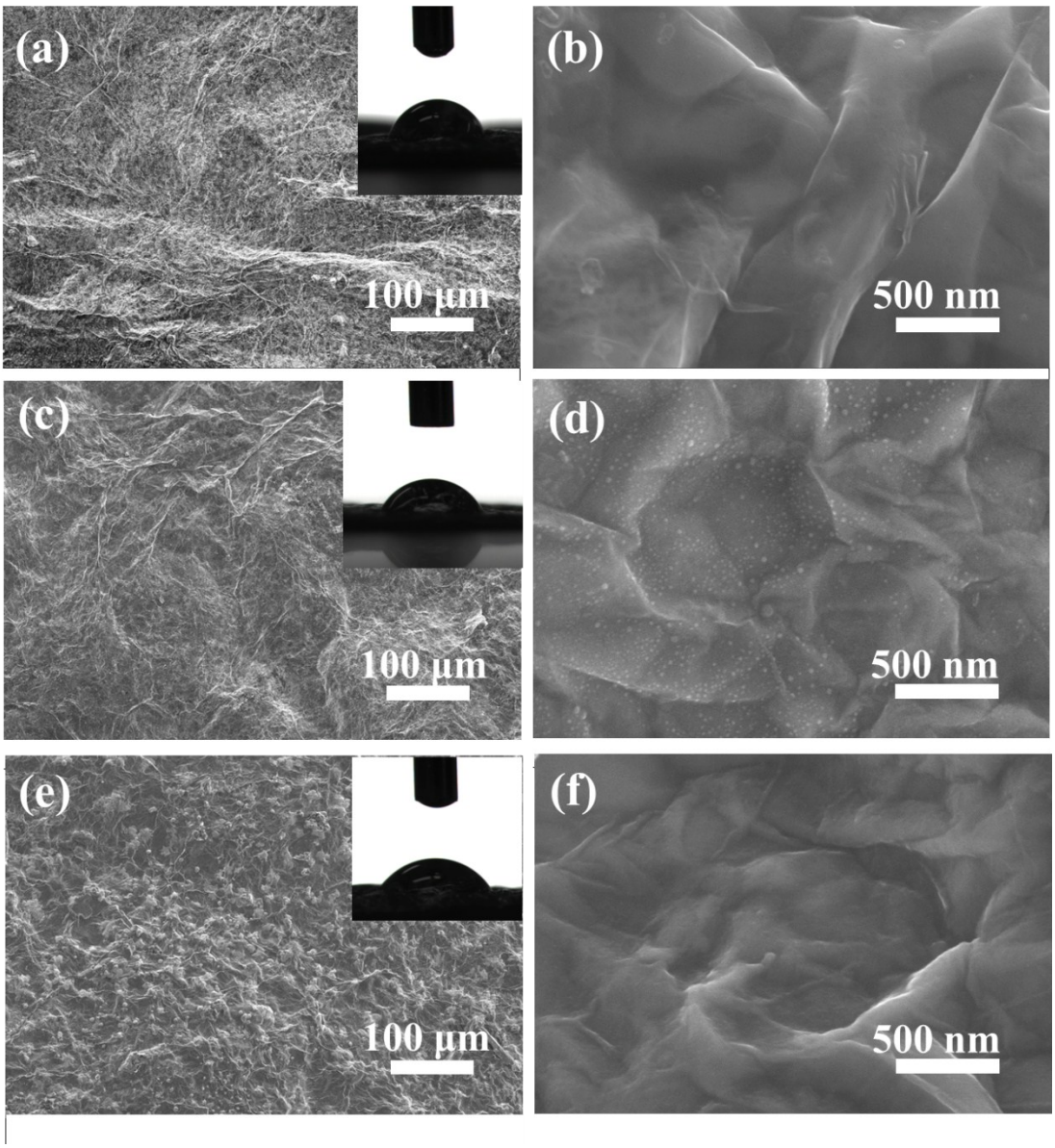

Figure S3 SEM images of MORGO-2 (a-b), MORGO-5 (c-d) and MORGO-15 (e-f) film with contract angel.

Note to Figure S3:

The effect of oxidation time on the microstructure and surface topography of RGO film was also investigated in more detail and the SEM images at different oxidation time were shown in Figure S. With the oxidation time increased from 2 to 15 min, the grooves and embossments on the surface become deeper and clearer due to the ongoing redox reaction between RGO film and the mixed acid.

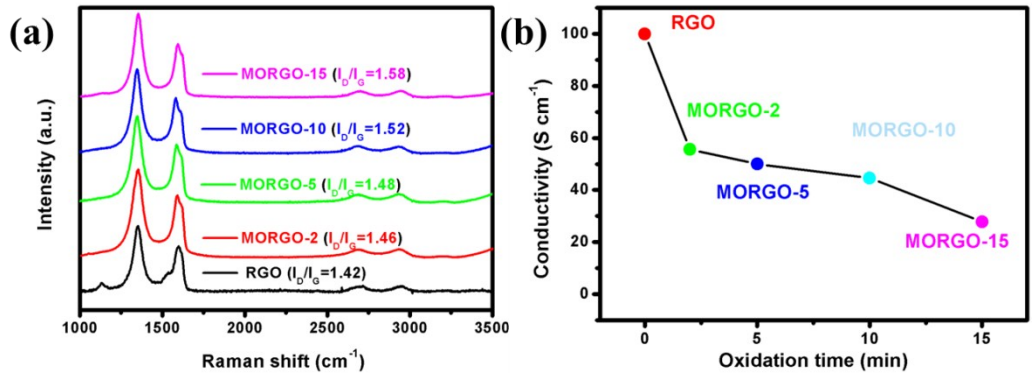

Figure S4 Raman spectra (a) and conductivity (b) of MORGO-X (X=2, 5, 10, 15) films.

Note to Figure S4:

The controllability of this electrochemical oxidation process was also studied. The ratio of I_D/I_G of MORGO-2, MORGO-5, MORGO-10 and MORGO-15 was 1.46, 1.48, 1.52 and 1.58, respectively, indicating more defects were created with the extended oxidation time. The increase in ratio is attributed to the smaller average size and the larger amount of new isolated graphitic domains that are created in the process of oxidation.[S. Stankovich, D. A. Dikin, R. D. Piner, K. A. Kohlhaas, A. Kleinhammes, Y. Jia, Y. Wu, S. T. Nguyen and R. S. Ruoff, Carbon, 2007, 45, 1558]

The conductivity of the RGO film is a function of the oxidation time (Figure). The RGO film exhibited the maximum conductivity of 100 S cm-1 and the electric conductivity decreases gradually after the electrochemical oxidation. The conductivity slightly decreased when the oxidation time increased from 2 to 10 min, but a drastic decrease was observed when time prolonged up to 15 min. The order of conductivity is RGO (100 S cm^{-1})> MORGO-2 (55.6 S cm^{-1}) > MORGO-5 (50 S cm^{-1}) > MORGO-10 (44.6 S cm^{-1}) >MORGO-15 (27.8 S cm^{-1}).

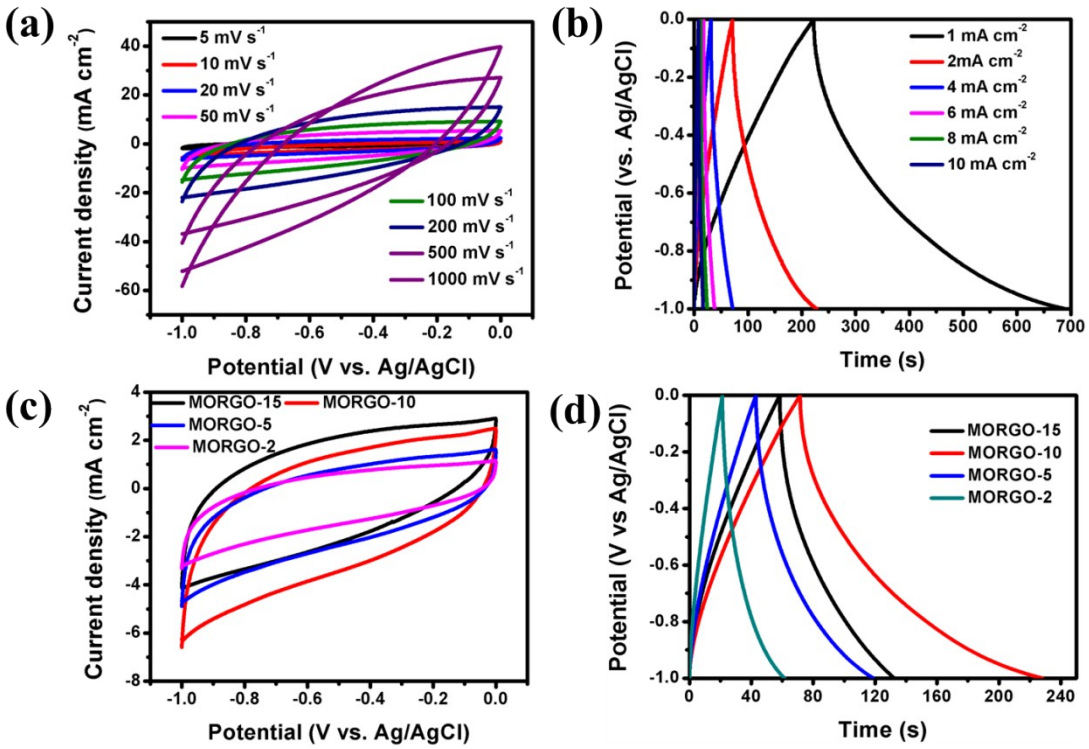

Figure S5 (a) CV and (b) GCD curves of MORGO under different scan rates and current density; (c) CV and (d) GCD curves of MORGO-X under 20 mV s^{-1} and 2 mA cm^{-2}, respectively.

Note to Figure S5:

The CV curves of MORGO collected at various scan rates from 5 to 1000 mV s^{-1} exhibited obvious rectangular shape as shown in Figure S5a. Even at a very high scan rate of 1000 mV s^{-1}, CV curves remain quasi-rectangular, indicating the superior rate capability and excellent frequency response. The GCD curves of MORGO at various current densities (Figure S5b) shows linear behavior and nearly symmetric shape, which confirm the ideal capacitive behavior. Figure S5c shows the CV curves of MORGO electrodes with different oxidation time at the scan rate of 20 mV s^{-1}. With the oxidation time increasing from 2 to 15 min, more and more oxygen functional groups were introduced into the edge sites of RGO sheets, and the current density of the CV curves gradually increased, indicating that the content of oxygen groups play an important role in providing high pseudocapacitance. It is worth mentioning that oxidized RGO for 2-10 min still have necessarily conductive network which could drive the redox reactions of oxygen functional groups. However, the MORGO electrodes exhibit a decreased

current density and irregular CV shape when with further prolongation of oxidation time from 10 to 15 min, which suggests that excessive functional groups will lead to an inferior capacitance performance. Similar conclusion is obtained from GCD measurement. Although the content of oxygen groups of MORGO-15 is much higher than MORGO-10, the conductive network is destroyed. The MORGO-15 exhibited a decreased current density, which suggests that appropriate quantities of the oxygen functional groups are essential to optimize the electrochemical performance of the RGO.

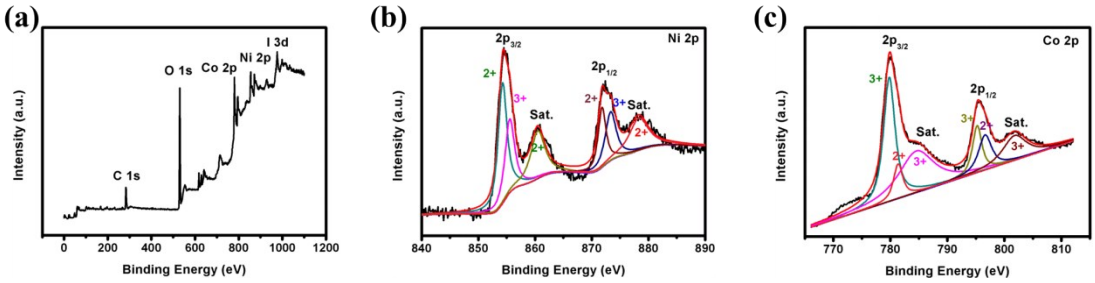

Figure S6 (a) Survey and high resolution (b) Ni 2p and (c) Co 2p XPS spectrum of the MORGO/NiCo-LDH.

Note to Figure S6:

XPS measurement was employed to probe the surface composition and chemical states of the as-made MORGO/NiCo-LDH, of which the detailed results are shown in Figure. It can be clearly seen from the survey spectrum (Figure) that the MORGO/NiCo-LDH consists of the C, O, Ni and Co as well as I elements which come from the reduction process of GO. By Gaussian fitting method, the spectrum of Ni 2p emission spectrum was best fitted with two obvious spin-orbit doublets along with two shake-up satellite peaks at 860.5 and 878.3 Ev (identified as "Sat."). The peaks at 854.3 eV and 871.8 eV can be assigned to Ni^{2+}, while the peak at 855.5 and 873.3 eV are attributed to Ni^{3+}. The Co 2p emission spectrum was also fitted with two spin-orbit doublets, in which the peaks at 781.4 eV and 795.2 eV can be assigned to Co^{2+}, while the peaks at 779.8 and 796.6 eV are attributed to Co^{3+}. Besides, two couple of shakeup satellite peaks at 784.6 and 801.8 eV represent the Co^{2+}. These results show that the chemical composition of NiCo-LDH contain Ni2+, Ni3+, Co2+ and Co3+, which are in good agreement with the results in the literature for NiCo-LDH.[Electrochimica

Acta 236 (2017) 18–27; Carbon 110 (2016) 1-7] The high-resolution spectrum for O1s consists of three oxygen species located at 529.2 eV (O1), 529.9 eV (O2) and 530.8 eV (O3). Specially, the O1 and O2 peaks at 529.2 and 529.9 eV is related to metal-bonded hydroxyls, while the O3 peak at 530.8 eV is associated with the physi- and chemisorbed water,[ACS Appl. Mater. Interfaces 6 (2014) 2450–2458; ACS Nano 7 (2013) 5430–5436.] further confirming the formation of NiCoLDH.

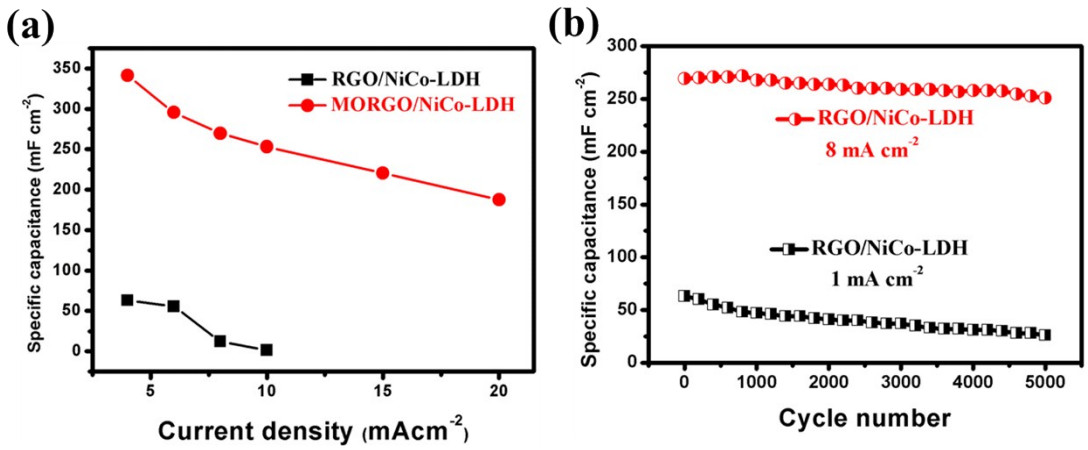

Figure S7 Comparison of the specific capacities (a) and cyclic life (b) of RGO/NiCo-LDH and MORGO/NiCo-LDH films electrode.

Note to Figure S7b:

To investigate the cyclic stability of the as-prepared RGO/NiCo-LDH and MORGO/NiCo-LDH, GCD test was repeated at a constant current density of 8 mA cm^{-2} for 5000 cycles. The RGO/NiCo-LDH exhibits a sharply capacitance decrease during the cycling process due to the poor affinity of NiCo-LDH and the RGO sheets. In contrast, the MORGO/NiCo-LDH shows excellent cycling stability with only 7% decrease of capacitance at a constant current density of 8 mA cm^{-1} after 5000 cycles. It is believed that the formation of C-O-Metal bonding between MORGO sheet and NiCo-LDH helps to retain the structural integrity, and thus could effectively suppress the structural breakdown of NiCo-LDH nanosheets during charge/discharge.

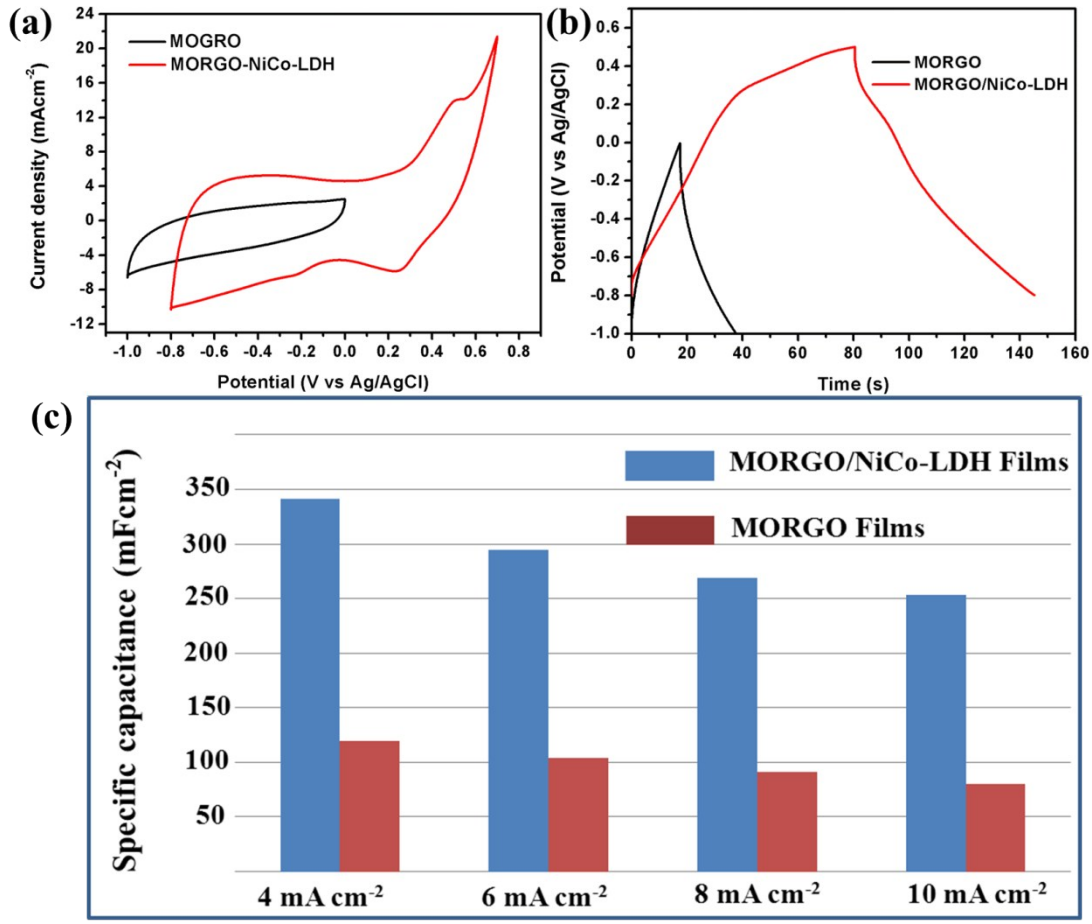

Figure S8 The comparison of CV curves (a) at 20 mV s^{-1} and galvanostatic charge/discharge curves under 6 mA cm^{-2} for MORGO films and MORGO/CoNi-LDH films; (c) the specific areal capacitance values of MORGO films and MORGO/CoNi-LDH films as a function of current densities.

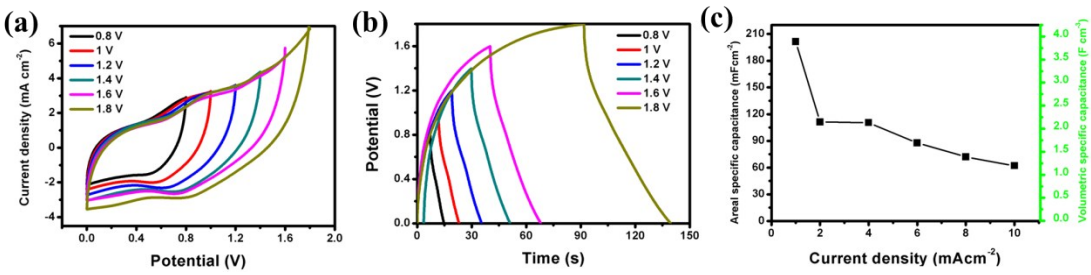

Figure S9 (a) CV and (b) GCD curves of the SSC device collected at various scan voltage in 20 mV s^{-1} and 2 mA cm^{-2} respectively. (c): The areal and volumetric capacitance values as a function of various scan rates for the all-solid-state SSCs were calculated. The maximum volumetric capacitance of the device can reach 4 F cm^{-3} at 1 mA cm^{-2}.

Table S1 Summary of some basic properties of various Asymmetric and Symmetric energy storage devices

Electrode materials	Electrolyte	Area capacitance (mF cm-2)	Dynamic conditions	Ref.
Vacuum-assisted thermal reduction RGO	H_3PO_4/PVA	0.678	1.5 uA cm^{-2}	38
Hirerarchical porous RGO films	H_2SO_4/PVA	37.95	0.6mA cm^{-2}	39
Honeycomb-like RGO	H_2SO_4/PVA	55.4	5mV s^{-1}	40
Microporous/mesoporous RGO	1M H_2SO_4	71	1mA cm^{-2}	41
Spontaneously reducing/assembling RGO films		124	1 mA cm^{-2}	42
RGO/PANI	H_2SO_4/PVA	6.4	0.08mA cm^{-2}	49
RGO-CNT	[EMIM][TFSI] gel electrolyte	33	1mA cm^{-2}	50
RGO-CNF	1M H_2SO_4	81	1mV s^{-1}	51
Graphene/PPy	0.1M $LiClO_4$	151	10 mV s^{-1}	52
RGO/*c*MWCNT	KCl	198.5	1mA cm^{-2}	53
MORGO	1M KOH	222	1 mAcm-2	**This work**
MORGO-NiCoLDH	1M KOH	341	4 mAcm-2	**This work**